



FORMULATION AND EVALUATION OF NANOPARTICLES OF ETOPOSIDE

¹Arun Mante , ²Dr. Laxmikant Barde

¹Research Scholar, ²Supervisor

^{1,2} School of Pharmacy, SunRise University, Alwar, Rajasthan, India

Corresponding author email:-mantearun11@gmail.com

ABSTRACT:

The present study functionalized MSNs as oral as well as intravenous targeted delivery agents for ETO in cancer therapy. MCM-41 mesoporous silica nanoparticles were synthesized based on the template synthesis method. The nanoparticles were evaluated for drug loading, in vitro dissolution, in vitro diffusion and characterized by FTIR, DSC, X-ray diffraction, SEM and TEM analysis. A similar pattern was obtained in ETO-loaded MSNs. This could be attributed to a complete encapsulation of ETO into the silica pores. no endothermic transition was observed in the thermogram corresponding to the ETO: MCM-41 mass ratio of 1:1.5. and similar for ETO-MCM-41-A, ETO-PAA-MSN and ETO-FA-MSN as well. Also, the XRD pattern obtained for MCM-41, MCM-41-A, PAA-MSN and FA-MSN NPs was amorphous. The obtained XRD results augmented those obtained from thermal analysis.

There was an evident increase in size with surface coating. PA-MSNs and FA-MSNs were seen to be well ordered with honeycomb like structure evident of well-preserved mesoporous characteristics post functionalization. The remarkable improvement in dissolution could be credited to the mesopores of MSNs converting the crystalline state of ETO to a non-crystalline state, which is well known for improving the dissolution rate.

Hence, FA-MSNs can be effectively used for targeting cancer cells which or intracellular components like lysosome and endosome possessing lower pH than the normal healthy tissue.

Keywords: cancer, nanoparticles, mesoporous, silica

INTRODUCTION:

Cancer is one of the most complicated genetic diseases affecting humans and one of the major causes of death worldwide. It is caused by the damaged cells proliferating out of control as a result of underlying regulatory faults. Numerous variables contribute to cancer. On the other hand, the inactivation of tumor suppression genes like p53 and the activation of oncogenes are the two main causes of the transformation of normal cells into cancer cells (4). Genetic mutations can arise from scratch, be inherited, be brought on by a virus, be brought on by exposure to carcinogens in the external environment, or even be the result of age-related genetic instability.

In 2019, 17,62,450 new cases of cancer are estimated and 6,06,880 cancer deaths are projected (8). It is also reported that prostate cancer has an occurrence rate 1 amongst every 5 new diagnosis. With such a high occurrence rate and being these cond leading cause of cancer related deaths in men(9), it become simperative to find a sure shot cure for the same.

ETO comes under the Biopharmaceutics classification system (BCS) class IV and suffers from solubility as well as permeability limitations. This leads to solubility and bioavailability issues. Formulating a novel drug delivery system can help in addressing various issues related to this drug. In this research work, an extensive investigation was carried out to determine the efficacy of mesoporous silica nanoparticles MCM-41 in particular in functioning as a delivery system for ETO. Their impact on the solubility and bioavailability of the drug was assessed. For oral delivery unfunctionalized MSNs and amine functionalized MSNs both were tested and comparison was made to determine effect of functionalization on ETO release and efficacy.

Thus, in the present chapter the application of bare and functionalized MSNs as oral as well as intravenous targeted delivery agents for ETO in cancer therapy have been discussed in depth along with their biosafety aspects and efficacy.

MATERIAL AND METHODS



MATERIAL

Pure anhydrous active pharmaceutical ingredient (API) Etoposide (ETO) was obtained as a sample gratis from Intas Pharmaceuticals Ltd, (Ahmedabad, Gujarat, India). Other Chemicals required were purchased from S.D. Fine Chem Ltd, Mumbai.

METHOD

Synthesis of bare MCM-41 type of MSNs

MCM-41 mesoporous silica nanoparticles were synthesized based on template synthesis method with few alterations (1). For the fabrication of MSNs, 2.21 grams (g) of CTAB playing a role of structural template was dissolved in de-ionized water and blended for 5 minutes (min).

3.24 milli liters (mL) of TMAOH was added to the reaction blend drop wise under continuous magnetic stirring. Later, 3g fumed silica was added after a time interval of 10 min. Finally, this was subjected to hydrothermal treatment for 48 h at 383K. The slurry obtained was filtered and dried appropriately. The synthesized MSNs obtained in the form of dry powder were subjected to calcination at 823K for 6h to completely evacuate the template.

Drug loading was achieved by novel immersion solvent rotary evaporation method (22). Butchi™ Rotary evaporator was used for evaporation of solvent during drug loading. ETO was dissolved completely in methanol in an RBF. Further individual addition of MCM-41, MCM-41-A, PAA-MSN, FA-MSN to the flask in the drug: carrier mass ratio 1:1.5. This was subjected to continuous stirring for 4h. After this the solvent was evaporated by rotary evaporator and a fine dried powder of ETO loaded MSNs was obtained. The final products were labelled as ETO-MCM-41, ETO-MCM-41-A, ETO-PAA-MSN, ETO-FA-MSN. Drug Loading and entrapment were calculated by UV-Vis at 285nm.

To ensure complete entrapment of drug into the mesopores FT-IR spectra of bare mesoporous carriers and synthesized MCM-41, MCM-41, MCM-41-A, PAA-MSN, FA-MSN and drug loaded; ETO-MCM-41, ETO-MCM-41-A, ETO-PAA-MSN, ETO-FA-MSN, BIC-MCM-41, BIC-MCM-41-A, BIC-PAA-MSN and BIC-FA-MSN were compared.

Differential scanning calorimetry (DSC) analysis:

Melting point and loading were determined by DSC Shimadzu-TA60 thermal analyzer equipped with the TA60-WS software. The heating rate was kept at 10°C/min. The existence of ETO and BIC on silica matrix in amorphous or crystalline form and complete encapsulation was further confirmed by DSC. Absence of any melting point depression is indicative of presence of drug in non-crystalline state in pores (8). Melting points of ETO and BIC were determined individually. DSC analysis of ETO-MCM-41, ETO-MCM-41-A, ETO-PAA-MSN, ETO-FA-MSN, BIC-MCM-41, BIC-MCM-41-A, BIC-PAA-MSN, BIC-FA-MSN was done and absence of any crystalline sharp drug peaks was ensured.

X-Ray diffraction analysis (XRD)

EMPYREAN, PANalytical model equipped with Cu K radiation beam operating at 40 kV and 40 mA was used to determine low angle X-Ray powder diffraction (LXD) pattern. The structure of pores was ascertained by low-angle XRD measurements. The spectra was an indication of the intactness of the mesoporous structure. XRD measurements were taken for MCM-41, ETO-MCM-41, MCM-41-A, ETO-MCM-41-A, PAA-MSN, ETO-PAA-MSN, FA-MSN and BIC-MCM-41, BIC-MCM-41-A, BIC-PAA-MSN and BIC-FA-MSN.

Morphological characterization was performed using scanning electron microscopy (SEM) (FEI-Quanta 200 operating at 20 kv) (Thermo Scientific, USA). The samples were coated with gold to make them conducting before imaging. TEM images were resolved over a photographic film taken on a TEM MCM-200 (Philips, India) model operated at 200kV voltage with a resolution of 2.4 Å. The images were resolved over a photographic film. SEM analysis was done to determine morphological and internal structure of bare MCM-41 and functionalized PAA-MSN and FA-MSNs respectively.

Zeta potential and size determination:

Particle Z-average size and charge were measured using dynamic light scattering (DLS) and electrophoretic mobility measurement (respectively), using the Malvern Zetasizer Nano ZS (Malvern Instruments, Malvern, UK). Zeta potential indicates the surface residual charge of the particles. The zeta potential measurements were done for MCM-41, MCM-41-A, PAA-MSN, FA-MSN and drug loaded MCM-41, MCM-41-A, PAA-MSN and FA-MSN.



In vitro release study:

The drug release pattern was determined and cumulative drug release was calculated for all the mesoporous formulations of ETO. For formulations to be administered by oral route, dissolution study was performed. Additionally, simulated and relevant media was used to study the effect of enzymes and food on drug release. For parenteral formulations, in vitro diffusion study was performed at different pH values using a medium.

In vitro dissolution study

Dissolution study was performed using Veego USP type II dissolution apparatus in 900 mL dissolution media at 50 rpm maintaining temperature of dissolution medium at $37 \pm 0.5^\circ\text{C}$. The *in vitro* release study was performed for plain ETO (API), MF, ETO-MCM-41 and ETO-MCM-41-A in acetate media (pH 4.6), simulated gastric fluid (SGF) (pH 1.2) and simulated intestinal fluid (SIF) (pH 6.8) containing pepsin and pancreatin respectively. Enzyme free SGF (pH 1.2) and SIF (pH 6.8) were also taken to study the presence of any interaction between hard gelatin capsule shell and amine group of MCM-41-A and whether it has any effect on the release of ETO. The drug release pattern was also studied in the presence and absence of food as well. Hence, the fed and fasted state simulated gastric and intestinal media were prepared (FaSSGF, FeSSGF, FaSSIF, FeSSIF) for this purpose. The composition of all media is summarized in Table 6.1 (23, 24). The powder was filled in the hard gelatin capsule shell prior to dissolution study. 5 mL aliquots were withdrawn at 5, 10, 15, 20, 30, 45, 60, 90, 120, 180, 240, 320 and 360 min intervals. The withdrawn samples were filtered through 0.45 μm PVDF filter membrane and analysed by UV spectrophotometer at 285 nm. Sink conditions were maintained throughout the study by adding an equivalent amount of fresh medium as that of withdrawn sample.

Dissolution Kinetic study

For the purpose of quantifying the differences in the release profiles of ETO formulations. The drug release data from both MCM-41 and MCM-41-A nanoparticles was fitted to various kinetic models and the best fit was determined. Different parameters by fitting the experimental data to different release models were calculated. Criteria for judgement on best model included lowest AIC (Akaike information criterion), highest MSC (Model selection criterion) and Regression values (R^2) (25). The various release model to which dissolution data were fitted include zero order, first order, Higuchi, Weibull, Hixon-Crowell and Korsmeyer-peppas model (26).

In vitro diffusion study

In the *in vitro* drug release study, a suspension of ETO, and ETO-MCM-41, ETO-MCM-41-A, ETO-PAA-MSN and ETO-FA-MSN was filled into a dialysis tube (cutoff Molecular weight (Mw) = 7000 g/mol for PAA-MSNs) and (cut-off Mw = 3500 for FA-MSNs). Further, the bag containing filled dispersion was then immersed into 100 mL (Phosphate buffer saline) PBS solution of different pH (5.5, 6.8 and 7.4) with continuous magnetic stirring at room temperature (RT). The samples were withdrawn at 2, 4, 8, 10, 12, 24, 30, 36, 48, 54, 60 and 72 h time intervals while maintaining adequate sink conditions to continue the release profile of drug. The samples were filtered through 0.22 μm membrane filter prior to analysis. The drug release at particular time intervals was calculated by measuring fluorescence intensity by a Spectrofluorophotometer with excitation wavelength fixed at 247 nm and emission measured at 323 nm.

Diffusion Kinetic study

The experimental data obtained from diffusion study was fitted to, zero order, first order, Higuchi and Korsmeyer-peppas kinetic model to determine the release mechanism for ETO. The data was fitted to appropriate model to determine the n value and in turn the release mechanism. DD-solver; an excel-addin was used for this purpose.

Result and Discussion

Fourier transform-Infrared (FT-IR) spectroscopy studies

FT-IR is useful in qualitative estimation for the identification of functional groups present. In FT-IR spectra of ETO (Fig 6.1(a)) showed several characteristic bands. The band corresponding to C-H stretch was observed at 2950 cm^{-1} . C=O stretch for ester and carboxymethyl was obtained at 1752 and 1610 cm^{-1} respectively. The C-O-C stretch was observed with bands observed at 1034 cm^{-1} . Bands obtained at 1478 and 1426 cm^{-1} could be attributed to the C=C stretching in the backbone of the aromatic phenyl ring.

All the MSN spectra exhibited bands that are characteristic of mesoporous silica (Fig 6.1). In FT-IR spectra of MCM-41, the typical bands at 811 cm^{-1} and 1085 cm^{-1} could be attributed to bending and asymmetric stretching of Si-O bonds. The vibrational band at 965 cm^{-1} is a characteristic feature of Si-

OH group routinely observed in silica material. The broad band pivoted at 3439 cm^{-1} is attributed to the hydroxyl stretching (O-H) due to the silanol groups. The number of CTAB present in asynthesized MSNs is typical C-H stretching vibrations at 2954 and 2898 cm^{-1} and C-H deformation vibration at 1452 cm^{-1} . However, after evacuation of CTAB all the bands occurring due to the presence of surfactant disappeared. Newer bands in the spectra of MCM-41-A stipulate the successful incorporation of the amine groups via functionalization. During surface decoration of MCM-41, the hydroxyl groups present on the surface of mesoporous silica react with APTES resulting in the formation of Si-O-Si bonds. The reduction in hydroxyl group is evidence of anchoring mechanism being involved in the reaction between silanol groups and APTES (29). A new band allocated to asymmetric bending of -NH_2 was observed at 1590 cm^{-1} . Moreover, a couple of bands assigned to CH_2 stretching were obtained at 2870 and 2930 cm^{-1} . Additionally, the prominent NH stretching mode can be observed at 3340 cm^{-1} . Moreover, there was a decrease in intensity of Si-O-Si stretching band at 1085 cm^{-1} in case of MCM-41-A, indicating a lower amount of silanol groups caused by attachment of NH_2 groups to the surface of silica. The existence of these peaks, altogether confirm the success of functionalization strategy. Successful functionalization with PAA was confirmed by new adsorption peaks appearing at 1551 , 1650 and 1714 cm^{-1} assigned to N-H bending, C=O stretching vibration in amide group and C=O stretching vibration in carboxyl group respectively.

The drug loaded FT-IR spectra of both MSNs exhibit a completely resolved peak of mesoporous silica. Additionally, most of the characteristic peaks of the drug are either not well visible or completely disappeared, due to fine housing of drug into MSN pores rather than on the surface. A similar pattern was obtained in ETO loaded MSNs. This could be attributed to a complete encapsulation of ETO into the silica pores.

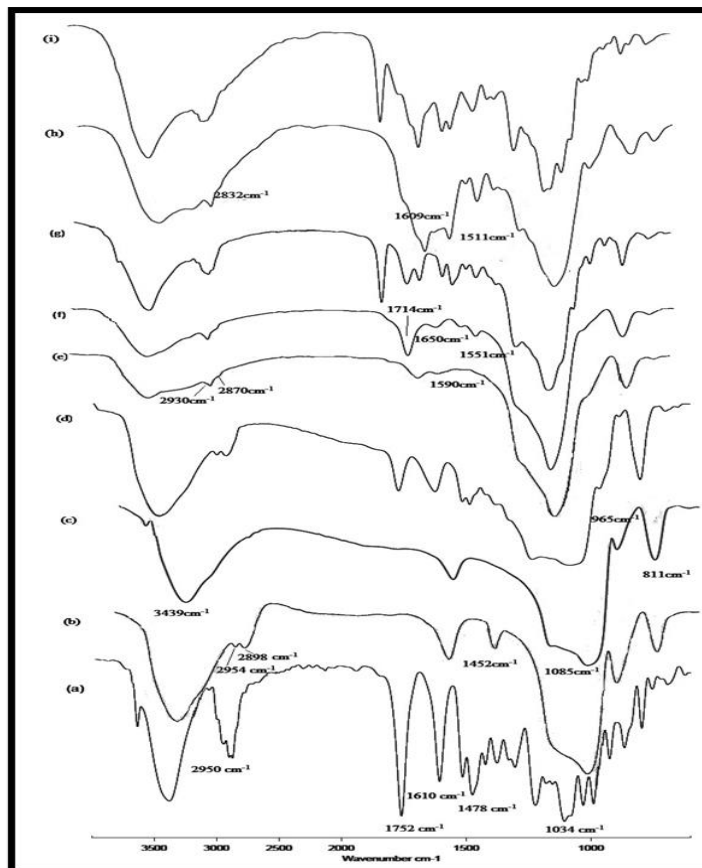


Figure 1. FT-IR Spectra (a) ETO (b) Asynthesized MSN (c) MCM-41 (d) ETO-MCM-41 (e) MCM-41-A (f) PAA-MSN (g) ETO-PAA-MSN (h) FA-MSN (i) ETO-FA-MSN

Differential scanning calorimetry(DSC)analysis

The DSC curve of ETO showed a stationary endothermic peak at 281.83°C (Fig 6.2 (a)), owing to its intrinsic melting point. If the drug is present in the crystalline form in the mesopores, the quantity of drug can be differentiated and calculated from the melting point depression by DSC. Absence of any melting point depression is indicative of presence of the drug in non-crystalline state in pores (30). Thermograms of all ETO-loaded MSNs were recorded and signals due to melting were noted. Notably, no endothermic transition was observed in thermogram corresponding to the ETO: MCM-41 mass ratio of 1:1.5 and similar for ETO-MCM-41-A, ETO-PAA-MSN and ETO-FA-MSN as well.

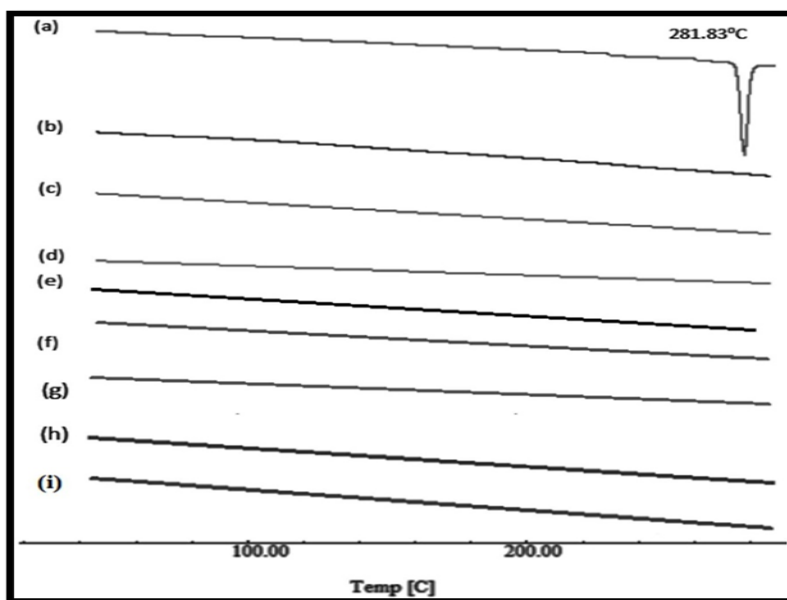
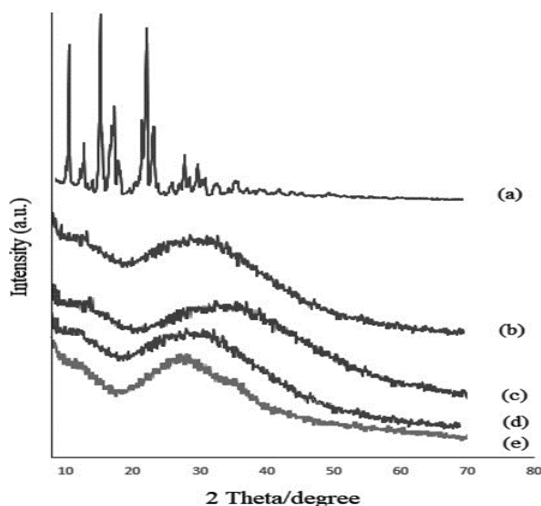


Figure 2. DSC thermograms of (a) Crystalline ETO (melting point of drug), (b) MCM-41 (c) ETO-MCM-41, (d) MCM-41-A (e) ETO-MCM-41-A (f) PAA-MSN (g) ETO-PAA-MSN

X-Ray diffraction analysis(XRD)

The crystalline nature of etoposide was confirmed by wide angle XRD spectra (Six characteristic sharp and intense peaks were obtained at 10.9°, 16.5°, 19.9°, 21.3°, 24.1° and 25.9°). Wide-angle XRD patterns were registered to investigate if the crystalline phase of ETO could be detected. Nevertheless, no crystalline ETO was detected in ETO-MCM-41 and ETO-MCM-41-A, ETO-PAA-MSN and ETO-FA-MSN (Mass ratio 1:1.5). Absence of any characteristic peak in loaded carrier is indicative of the fact that ETO loaded into the MSNs was in a non-crystalline state. Also, the XRD pattern obtained for MCM-41, MCM-41-A, PAA-MSN and FA-MSN NPs was amorphous. The obtained XRD results augmented those obtained from thermal analysis.



Zeta potential and size determination:

Zeta potential indicates the surface residual charge of the particles. The zeta potential values of MCM-41 was found to be -36.86 mV. This can be attributed to the large number of silanol groups on silica surface (35). Loading of ETO into both MCM-41 and MCM-41-A gave zeta potential values of -37.25 and +29.40 mV respectively. However, loading of ETO did not alter the nature of surface charges in either case. The z average diameter was found to be around 110.2 nm for MCM-41 NPs and 124.7 nm for MCM-41-A NPs, as depicted in the graphs (Fig 6.6). The zeta potential values for ETO-MCM-41, ETO-MCM-41-A and ETO-FA-MSN were -37.25, 29.4 and 41.27 mV respectively. Z average diameter for MCM-41 and MCM-41-A was found to be 110.2 nm, 124.7 nm respectively. After functionalization with PAA, the value dropped to -31.15 mV due to the occurrence of large number of acidic carboxylic groups in polyacrylic acid. PAA decorated MSNs exhibited Z average diameter of 142.85 nm. FA-MSN exhibited z average diameter of 135.38 nm. There was an evident increase in size with surface coating.

SEM analysis:

The SEM micrographs divulge spherical morphology of synthesized particles MCM-41 NPs. There are certain limitations associated with SEM in giving a detailed in depth structure of the nanoparticle. Hence, additionally TEM analysis was also performed to ascertain the porous structure of MSN. Clear well defined Honey comb like hexagonal network was visible in the TEM images (Fig 6.9). MCM-41 TEM images were evidence that clear so structures were present in the samples and were still intact. PAA-MSNs and FA-MSNs were seen to be well ordered with honeycomb like structure evident of well-preserved mesoporous characteristics post functionalization.

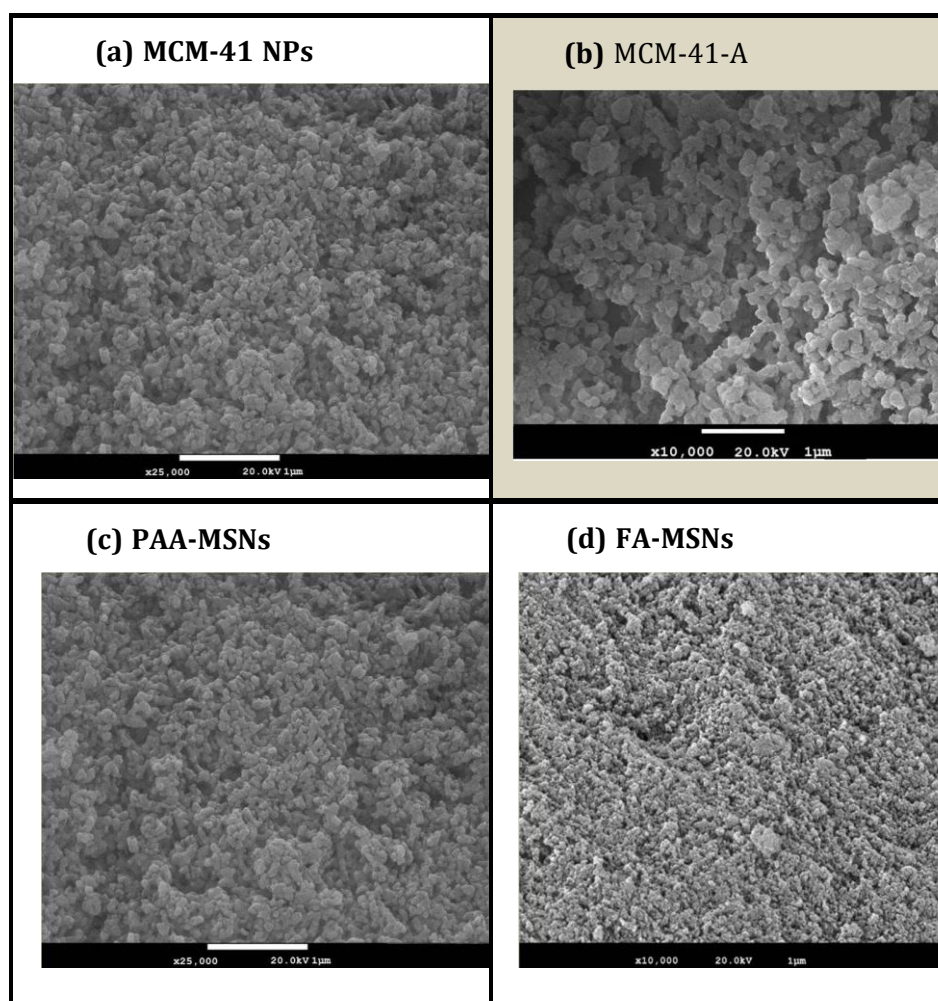


Figure 4. SEM images of MSNs (MCM-41 and surface functionalized MSNs viz, MCM-41-A, PAA-MSN, FA-MSN)

In vitro release study:

In vitro dissolution study

The dissolution profile of crystalline ETO, ETO-MCM-41, ETO-MCM-41-A and Marketed formulation (MF).

Appreciably, the rate of ETO release from MCM-41 was higher than that of plain crystalline ETO and MF. A remarkable dissolution enhancement of 5.1 times (from MCM-41) in comparison to plain ETO and 1.16 times in comparison to marketed formulation was obtained (at 45 min acetate media). Burst release was observed in case of unmodified MCM-41 with about 43 percent drug releasing in within the first 5 minutes, while when compared, a sustained release was obtained with MCM-41-A nanoparticles. This could be attributed to the fact that unmodified MCM-41 possess only silanol groups on the pore channel walls. These silanol groups form weak hydrogen bonds with ETO. To prevent this behaviour, the surface of MSNs was modified with amino groups on the pore channel walls. As evident, this provided a sustained release of ETO.

For Fickian diffusion ETO released is governed by diffusion and solvent transport rate or diffusion is much greater than the process of polymeric chain relaxation. Moreover, if n value is greater than unity, it signifies Super case II model (39). Thus, it can be assumed that for PAA-MSN the anomalous mechanism based drug release is controlled both by diffusion and polymer swelling. Furthermore, in case of ETO-MCM-41, not much pronounced pH dependent release was observed, and the mechanism of release was Fickian. Thus, it could be observed that a pH selective and effective sustained release was obtained in case of ETO-MCM-41-PAA for greater than 72 h. A complete summary of release mechanisms is given in table 6.7.

High payload of ETO was obtained for FA-MSNs. The *in vitro* release profile of drug in different pH conditions exhibited a different behavior (Fig 6.13). ETO-MCM-41-A and ETO-FA-MSNs showed a pH-dependent release pattern in neutral and acidic PBS. A more responsibility was observed in case of FA-MSN. However, ETO-MCM-41 were devoid of any pH responsive behaviour and did not give a differential release pattern. The release of ETO was found to be inversely proportional to pH in case of FA-MSN. More of ETO was released in acidic media as compared to higher media. Hence, FA-MSNs can be effectively used for targeting cancer cells which or intracellular components like lysosome and endosome possessing lower pH than the normal healthy tissue.

CONCLUSION:

The results obtained from the entire study suggested that the ETO encapsulation into the MSN framework was successful and resulted in a marvelous enhancement in its dissolution rate (5.1 times) and bioavailability (4.35 times) in case of ETO-MCM-41. This in turn could lead to a significant dose reduction and it may be possible to achieve greater efficacy with the lowest dose of drugs that suffer from solubility and permeability limitations.

The most important aspect of a delivery system, the biosafety of MSNs was also established by hemolysis and histological examination. All the MSN formulations proved to be hem-compatible and safe. This property of MSNs can prove to be a benchmark in cancer treatment as it will prove to be less toxic on healthy human organs at the same time efficient in accumulating the dose in the tumor cells. This will lead to diminished toxicities and overcome the drawbacks associated with chemotherapy at a greater extent.

REFERENCE

1. Torre LA, Bray F, Siegel RL, Ferlay J, Lortet-Tieulent J, Jemal A. Global cancer statistics, 2012. *CA: a cancer journal for clinicians*. 2015;65(2):87-108.
2. Stewart BW, Wild C. World Cancer Report 2014. Lyon, France: International Agency for Research on Cancer, World Health Organization. 2014:630.
3. Zhang F, Li M, Wang J, Liang X, Su Y, Wang W. Finding new tricks for old drugs: tumoricidal activity of non-traditional antitumor drugs. *AAPS PharmSciTech*. 2016;17(3):539-552.
4. Kandoth C, McLellan MD, Vandin F, Ye K, Niu B, Lu C, et al. Mutational landscape and significance across 12 major cancer types. *Nature*. 2013;502(7471):333.
5. Jemal A, Siegel R, Ward E, Hao Y, Xu J, Murray T, et al. Cancer statistics, 2008. *CA: a cancer journal for clinicians*. 2008;58(2):71-96.
6. Program NCR. Three year report of population-based cancer registries: 2009–2011.
7. Indian Council of Medical Research, NCDIR-NCRP (ICMR) Bangalore; 2013.
8. Segal R, Miller K, Jemal A. *Cancer statistics, 2018*. *CA Cancer J Clin*. 2018;68:7-30.
9. Siegel RL, Miller KD, Jemal A. *Cancer statistics, 2019*. *CA: a cancer journal for clinicians*. 2019.
10. Miller B, Ries LG, Hankey B, Kosary C, Harras A, Devesa S, et al. *SEER cancer statistics review: 1973-*

1990. Bethesda, MD: National Cancer Institute. 1993;93:2789.
11. Frame I, Cant S. Current challenges in prostate cancer: an interview with Prostate Cancer UK. *BMC medicine*. 2015;13(1):166.
 12. Li F. Molecular epidemiology studies of cancer in families. *British journal of cancer*. 1993;68(2):217.
 13. Burks D, Littleton R. The epidemiology of prostate cancer in black men. *Henry Ford Hospital Medical Journal*. 1992;40(1-2):89-92.